Multi-Disk Coreless Axial Flux Permanent Magnet Synchronous Motors with Surface PM and Halbach Array Rotors for Electric Aircraft Propulsion

Matin Vatani
SPARK Lab, Pigman Eng. College
University of Kentucky
Lexington, KY, USA
matin.vatani@uky.edu

John F. Eastham
Dept. of Electronic & Electrical Eng.
University of Bath
Claverton Down, Bath, UK
jfeastham@aol.com

Dan M. Ionel
SPARK Lab, Pigman Eng. College
University of Kentucky
Lexington, KY, USA
dan.ionel@ieee.org

***Abstract*—This paper presents multiple single- and multi-disk coreless axial flux permanent magnet (AFPM) motors, focusing on specific power density and reliability for electric aircraft propulsion. Several 3D finite element analysis (FEA) parametric studies were conducted to assess the geometric impacts on a single-disk coreless AFPM motor featuring two separate stators and a double-sided Halbach array rotor configuration. These studies form the foundation for the design of both single- and multi-disk machines. Single-disk coreless AFPM motors with rotor back iron embedded between the stators, offering magnetically decoupled stators, are subsequently introduced. The paper concludes by presenting four multi-disk coreless AFPM motor topologies, comparing their electromagnetic performance and fault-tolerance capabilities.**

***Index Terms*—Axial flux PM machines, multi-disk AFPM, coreless AFPM, electric aircraft, Halbach array, number of poles, 3D finite element analysis.**

I. Introduction

The aviation industry currently contributes three percent of global CO_2 emissions. In addition, according to a forecast by Roland Berger [1], this share could rise to 24% by 2050 if other industries decarbonize as projected and no substantial technological advancements occur in aviation. To this end, the National Aeronautics and Space Administration (NASA) launched a collaborative academic and industrial framework under the University Leadership Initiative (ULI) for the Integrated Zero Emission Aviation (IZEA) project.

This initiative focuses on researching advanced technologies for a regional blended wing body aircraft with distributed hybrid hydrogen-electric propulsion, as outlined by Patel *et al.* [2]. The main specifications of the electric motor for this project are detailed by Vatani *et al.* [3], while this paper contributes to enhancing performance and reliability by employing multi-stage electric motors.

This project promotes powertrain systems and components, including electric motors, power electronics, and thermal management systems, to maximize specific power density and efficiency. As presented by Rosu *et al.* [4], achieving this requires multiphysics design optimization for the propulsion system at both the system and component levels.

Gieras *et al.* [5] and Nishanth *et al.* [6, 7] have demonstrated that axial flux permanent magnet machines (AFPMs) can be more power-dense than their radial flux counterparts. Additionally, the AFPM structure offers better cooling, enabling higher electric loading and improving torque capability. Taran *et al.* [8] have shown that the coreless stator variant of AFPM machines offers higher specific power and is potentially more efficient due to the elimination of core-associated losses. Furthermore, Chulaee *et al.* [9] showed that using a Halbach array rotor in coreless AFPMs can increase power by 40% within a constant motor envelope.

Examples of research on AFPM motors with Halbach array rotors for electric aircraft propulsion include an ultra-light-weight double-sided rotor and yokeless and segmented armature (YASA) machine by Talebi *et al.* [10, 11], a slotless stator with two radial rotors and one axial that uses three surfaces for torque production, by Du *et al.* [12, 13], and design consideration for coreless AFPM machines for high specific power and efficiency by Duffy *et al.* [14].

Axial flux machines enable the integration of multiple units on a single shaft, providing greater compactness compared to radial flux machines, which suffer from volumetric overhead due to their two sets of end windings. When the outer diameter is limited, stacking multiple AFPM units on a single shaft can meet the required power output. This configuration also enhances the propulsion system's reliability, as the decoupled electromagnetic units can continue operating at partial power even if some units fail.

Eastham *et al.* [15] pioneered the concept of multi-disk AFPM motors for unmanned electric aircraft in the early 2000s, designing a coreless AFPM machine with three stators and four rotors. More recently, Bingham *et al.* [16] set a world record for the fastest electric aircraft by using three YASA AFPM motors on a single shaft to drive the propeller.

In this paper, we propose and investigate four distinct multi-stator and multi-rotor (MSMR) AFPM motors featuring either fully coreless or stator coreless structures for electric aircraft propulsion systems. Section II details the sizing procedure for a single-disk coreless AFPM motor, providing the foundation

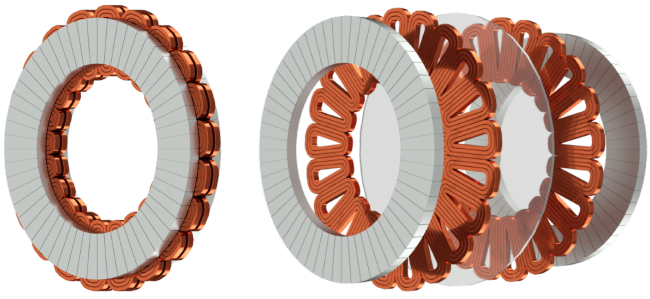

(a) (b)

Fig. 1. Single-disk coreless AFPM motor with Halbach rotors showing (a) compact and (b) exploded views

for developing multi-disk configurations. Section III introduces the four proposed multi-disk topologies and assesses their electromagnetic performance. Section IV explores the fault-tolerant capabilities of these motors in electric aircraft applications. Finally, Section V concludes the study.

II. Single-Disk Coreless AFPM Motor Topology and 3D FEA Parametric Studies

In this section, multiple parametric studies have been conducted to establish a primary design procedure for coreless AFPM motors with Halbach PM array rotors. These studies focus on a single-disk machine to ensure the findings are general and applicable to various MSMR configurations. The topology and design optimization of the single-sided motor, as outlined in [3], serve as the basis for these parametric studies and the development of MSMR topologies.

The single-disk machine, shown in Fig. 1, uses double-sided Halbach PM array rotors featuring two PMs per pole—one magnetized normally and the other tangentially to the airgap. This design eliminates the need for a ferromagnetic back plate as a flux return path, allowing it to be replaced with a much lighter and still robust material, such as carbon fiber.

The stator comprises two sets of electrically separated three-phase windings with a concentrated winding pattern. Each stator can be connected to a separate power electronics equipment and drive system, thereby increasing reliability. A space between the two stators is included to allow for direct cooling, enabling higher current density values.

The proposed single-disk coreless AFPM machine is designed to deliver a power output of 1.5 MW at 3,000 rpm, with a specific power density exceeding 10 kW/kg and an efficiency greater than 93%. The machine's outer diameter is set at 500 mm, aligning with the primary design specifications of the blended wing airplane body for this project [17].

Since AFPM machines involve complex 3D problems, accurate electromagnetic performance evaluations require a high computational burden 3D finite element analysis (FEA). Conducting parametric studies on all geometric parameters can be time-consuming. Analytical modeling, however, can provide valuable insights into the relationships between different parameters and their impact on the machine's performance, and can be considered for 3D FEA parametric studies. For a

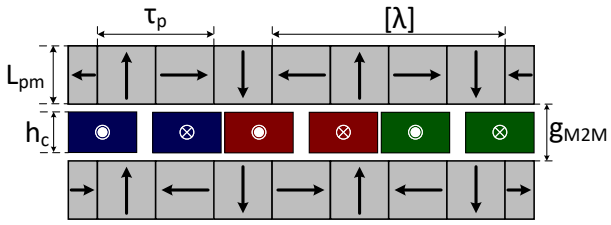

Fig. 2. A 2D view of geometric design variables through an axial cut at average diameter.

Table I
Geometrical independent variables and their corresponding limits employed for 3D FEA parametric study.

Parameter	Description	Min	Max
P	Pole number	8	48
$k_g = g_{M2M}/\tau_p$	M2M gap ratio	0.1	2
$k_{pm} = L_{PM}/\tau_p$	Magnet length ratio	0.1	2
$k_{rl} = (OD_r - ID_r)/\tau_p$	Radial length ratio	0.1	2.5

double-sided Halbach PM array, the airgap flux density can be calculated as follows [18]:

$$B_n = 2B_r \sum_{i=0}^{\infty} \frac{\sin(\epsilon n\pi/m)}{n\pi/m} \left[1 - \exp\left(\frac{-n\pi L_{pm}}{\tau_p}\right)\right] \exp\left(\frac{-n\pi g_{M2M}}{2\tau_p}\right) \cosh\left(\frac{n\pi y}{\tau_p}\right) \sin\left(\frac{n\pi x}{\tau_p}\right), \quad (1)$$

where B_r is the remanence of the PMs, ϵ usually set to one, $n = 1 + mi$, m is the number of PMs per wavelength, L_{pm} is the PM length, g_{M2M} is the PM-to-PM gap distance, and τ_p is the pole pitch.

The equation indicates that the effect of PM length and magnet-to-magnet gap depend on the pole pitch. L_{pm}/τ_p and g_{M2M}/τ_p define the geometry independent of scale. τ_p is determined by the number of poles within a constant outer diameter and rotor radial length. As the PM length increases, the flux density is enhanced, but the mass is higher. Regarding the magnet-to-magnet gap, increasing it reduces the airgap flux density but provides more space for conductors.

To determine the optimal geometric relationships for the Halbach array, a 3D FEA parametric study was conducted by varying one geometric parameter at a time. The results are presented in Fig. 3. Each subfigure examines specific power density, efficiency, and power by varying a single geometric parameter. The parameters and their values are shown in Fig. 2 and Table I.

The effect of PM length is analyzed in Fig. 3a, which shows that high values of specific power density are achieved for $L_{pm} = \tau_p \leq 0.4$. The power produced increases until it reaches $L_{pm} = 2\tau_p$. In this study, the ampere-turn and current density were kept constant, ensuring that the copper loss remained unchanged. Consequently, the efficiency improves as the power increases with larger magnet lengths.

In the M2M gap parametric study, g_{M2M} was increased up to $2\tau_p$ with the modification of ampere-turn according to

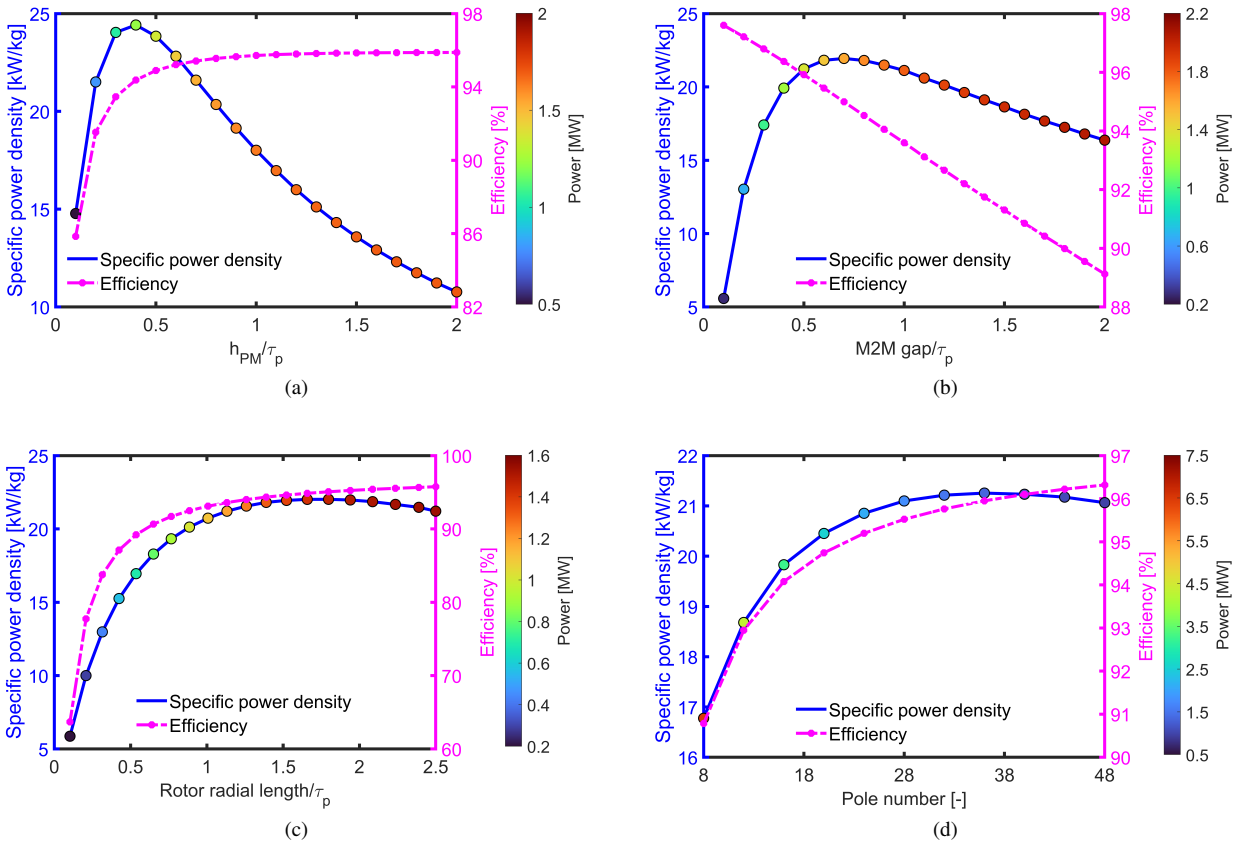

Fig. 3. Specific power density and efficiency 3D FEA parametric study results, showing for the variable (a) PM length, (b) magnet-to-magnet gap with modified amper-turn, (c) rotor radial length, and (d) pole number.

the available space in the airgap. The PM length was kept constant, so the changes in specific power density are due to the thicker coils. The parametric study results shown in Fig. 3b indicate that high values of kW/kg can be obtained with $0.5\tau_p \leq g_{M2M} \leq 0.6\tau_p$. However, the efficiency continuously decreases due to the greater number of turns in larger magnet-to-magnet gaps.

The parametric study results for various rotor radial lengths in the motor specifications are shown in Fig. 3c. The values of τ_p vary with different rotor radial lengths, so L_{pm} and g_{M2M} are adjusted to maintain their ratios over the pole pitch equal to 0.5. Both kW/kg and efficiency increase until $k_{rl} = \tau_p$, after which they experience saturation. For rotor radial lengths greater than one pole pitch, the produced power increases at the same rate as the machine's mass.

Based on the above results, the optimal geometric proportions of PM length, magnet-to-magnet gap, and rotor radial length relative to τ_p can be determined. These parameters can be scaled up as the pole pitch increases at lower pole numbers, thereby enhancing the magnetic and electric loadings.

The results of the pole number parametric study are presented in Fig. 3d. They show that specific power density improves up to a certain pole number, which depends on the machine's current density, speed, and outer diameter. However, beyond this point, the production of torque and power decreases as both magnetic and electric loadings diminish with higher pole numbers. An increase in pole number results in higher efficiency, as greater pole number leads to smaller M2M gaps and reduced copper losses.

For an example design, the Halbach array optimal geometric proportions for L_{PM}, g_{M2M}, and OD_r–ID_r were applied to a parametric FEA model. The pole count was varied to achieve a power output of 1.5 MW while maintaining a constant current density. With 20 poles, the proposed machine delivers the required power output of 1.5 MW and achieves a specific power density of 21.9 kW/kg.

Although this design meets the requirements of the NASA ULI IZEA project, a higher specific power density can be achieved with a greater pole count. The use of a multi-disk topology allows for an increased pole count while maintaining a constant outer diameter and a larger axial length. The following section of the paper explores various multi-disk coreless AFPM configurations and evaluates their performance.

III. Single-Disk Coreless AFPM Motors with Electromagnetically Decoupled Stators

The coreless AFPM motor depicted in Fig. 1 features two stators, each connected to its own inverter, ensuring electrical isolation between them. This design allows one stator and its corresponding inverter to continue functioning normally even if a fault occurs in a switch of the other inverter. However, the stators are magnetically coupled, meaning a fault in one stator will still impact the other.

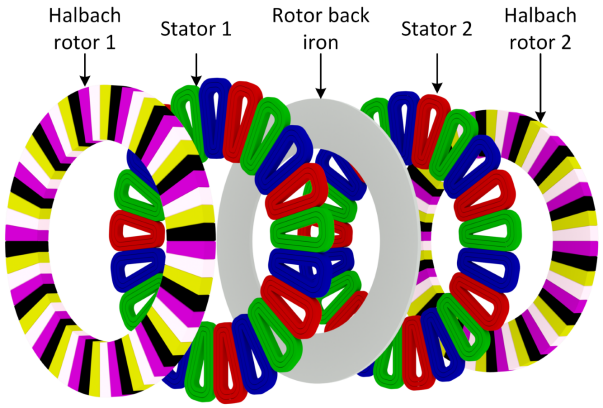

(a)

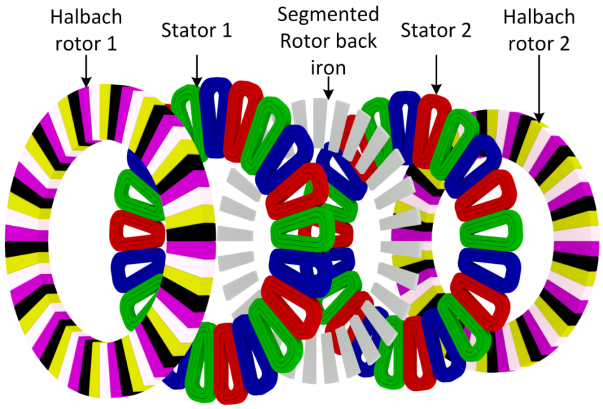

(b)

Fig. 4. Single-disk coreless AFPM motors with outer Halbach rotors: (a) with a disk rotor back iron and (b) with a segmented rotor back iron, positioned between the two stators.

Utilizing Halbach PM array rotors eliminates the necessity for rotor back iron to complete the flux path. However, incorporating a rotor back iron between the stators offers substantial benefits, such as reducing flux leakage, enhancing torque production, and achieving magnetic decoupling between the stators. These improvements stem from a more concentrated flux in the airgap when a ferromagnetic core is present.

The single-disk coreless AFPM motor featuring rotor back iron positioned between the stators is illustrated in Fig. 4. This ferromagnetic back iron can either be disk-shaped or consist of segmented structures embedded in non-ferromagnetic materials. Due to the axial direction of magnetic flux through the back iron, its axial length remains minimal. Although the M2M gap can remain unchanged with the addition of back iron, stator cooling becomes more challenging. This may require increasing the M2M gap to accommodate stator cooling solutions.

The electromagnetic performance of the proposed coreless AFPM motors, both with and without rotor back iron, are compared in Table II. Incorporating rotor back iron between the stators increases torque capability by approximately 5%. Among the designs, the motor with a segmented rotor back iron achieves the highest active specific power density, whereas the motor with a disk-shaped back iron has the lowest value.

Table II
ELECTROMAGNETIC PERFORMANCE COMPARISON OF CORELESS AFPM MOTORS WITH AND WITH ROTOR BACK IRON BETWEEN STATORS.

CAFPM Fig.	Power [MW]	Spec. power [kW/kg]	Mutual Induc. St 1 & St 2 [-]	Core loss [W]	Eff. [%]
1	1.51	21.9	$\approx \frac{1}{2}L_{aa}$	N/A	95.7
4a	1.59	19.2	≈ 0.0	790	95.9
4b	1.58	22.3	$\approx \frac{1}{3}L_{aa}$	590	95.9

A key benefit of adding rotor back iron is the magnetic decoupling between stators, which enhances the overall reliability of the propulsion system. Calculations of the mutual inductance between phases of different stators demonstrate that with disk-shaped back iron, complete decoupling of the stators is achievable. This decoupling not only shields one stator from faults occurring in the other but also protects the inverter.

In the 3D FEA models, the rotor back irons are assumed to be solid. As they rotate at synchronous speed and the harmonic flux density from the stator windings is minimal, core losses are negligible. The design with segmented back iron has an even lower core loss due to the reduced quantity of steel.

IV. Multi-Disk Coreless AFPM Motors and Electromagnetic Analysis

This section analyzes the electromagnetic performance of multi-disk machines, considering their efficiency, use of PM materials, goodness, and specific power density. The following section delves into the modularity introduced by the MSMR topologies and evaluates their fault-tolerant capabilities for electric aircraft applications.

The first MSMR topology is a two single-stator and double-rotor coreless AFPM machine with a surface-mounted PM rotor on one shaft, as illustrated in Fig. 5a. In the second topology, depicted in Fig. 5b, the middle rotors of type (a) are replaced with sets of normally magnetized PMs mounted on a non-ferromagnetic material. The middle rotor has the same pole count as the outer rotors but with a thicker PM length. The third and fourth machines have similar designs to types (a) and (b), but with the rotors replaced by consequent Halbach array poles. The machines are labeled as (a) to (d) in the caption of Fig. 5, and these labels will be used for reference throughout this paper.

The proposed coreless AFPM machines were designed based on the parametric studies outlined in Section II. For the Halbach array rotors, the PM length was set to half of the pole pitch, while for the surface PM variant, it was set to 0.3. PM width to pole pitch ratio was set at 0.8, and the back iron thickness was chosen to prevent core saturation. A consistent magnet-to-magnet gap of one pole pitch was maintained across all topologies. The rotor's radial length and the number of poles were treated as variables to ensure the machines produced a rated power of 1.5 MW.

A parametric study on pole numbers using 3D FEA has been conducted to compare the electromagnetic performance of four multi-disk topologies, as shown in Fig. 6. The pole

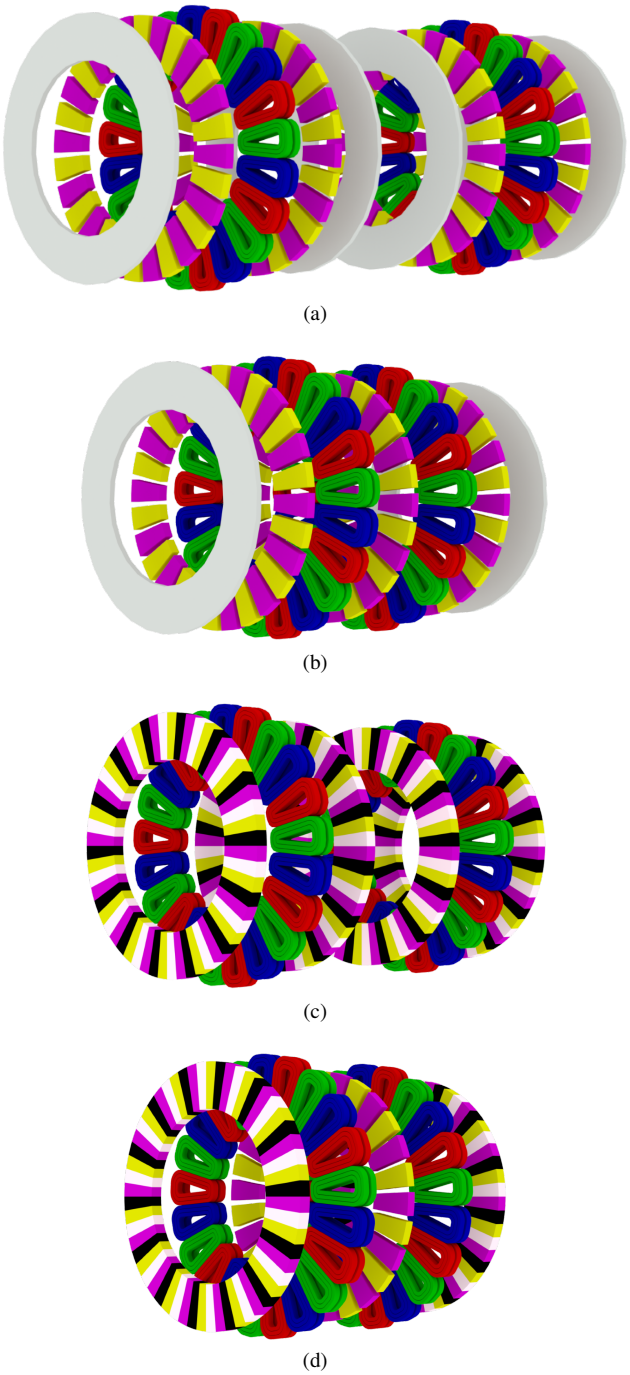

(a) (b) (c) (d)

Fig. 5. Multi-disk coreless AFPMs with (a) and (c) two independent single-disk machines and (b) and (d) outer surface PM or Halbach rotors and middle rotor with normally magnetized PMs.

number was varied from 24 to 40, with adjustments to current density to ensure a 1.5 MW power output for all designs. The results indicate that increasing the pole number improves specific power density. However, this also necessitates higher electric loading and current density, which reduces efficiency.

The multi-disk coreless AFPM motor of type (d) achieves the highest specific power density, while type (c) delivers the highest efficiency. Designs with the same pole count but different topologies, as shown in Fig. 6, have identical

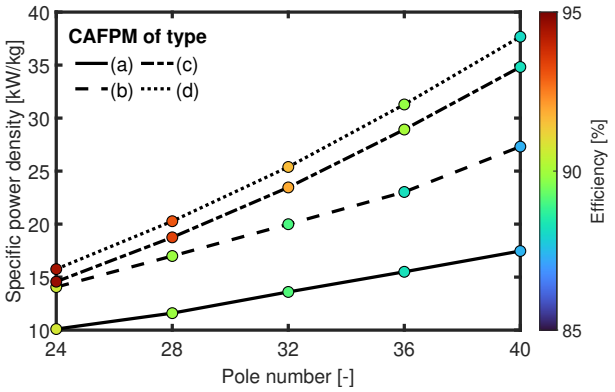

Fig. 6. Efficiency and specific power results for variable pole number. Other variables have been modified based on the pole pitch.

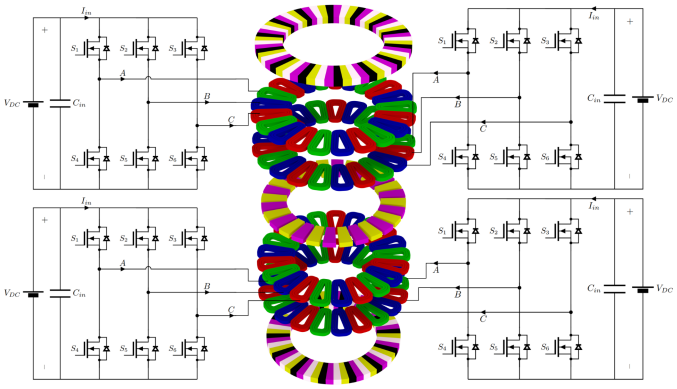

Fig. 7. The proposed multi-disk coreless AFPM motor features four electrically isolated stators, each powered by a separate inverter, thereby enhancing the overall reliability of the propulsion system.

copper mass. Therefore, variations in specific power density are attributed to the number of rotors and their configurations. Coreless AFPM motors with surface PM rotors exhibit lower specific power density and efficiency compared to those with Halbach array rotors.

The results in Fig. 6 show that MSMR topologies can achieve higher specific power densities by increasing the pole numbers, albeit at the expense of lower efficiency. To enhance efficiency in multi-disk topologies with high pole numbers, such as 40, the radial length of the machine can be increased, thereby improving magnetic loading. This permits a reduction in current density, which in turn increases efficiency. Table III lists designs with high efficiency values.

The relatively high current density values presented in Table III can be achieved with an advanced thermal management system, as detailed in [19]. Furthermore, ongoing thermal analysis of the proposed motor, utilizing computational fluid dynamics (CFD) methods, suggests that these current density levels are attainable with direct stator cooling at cryogenic temperatures, according to preliminary results.

V. Fault Tolerant Capability of Multi-Disk Coreless AFPM Motors

A crucial requirement for an electric aircraft propulsion system is fault tolerance. This can be accomplished through

Table III
PERFORMANCE COMPARISON OF THE MSMR CORELESS AFPMS. DESIGNS WERE SELECTED BASED ON THE RESULTS OF FIG. 6, IN WHICH K_{rl} WAS INCREASED TO IMPROVE THE EFFICIENCY.

CAFPM type	Pole num. [-]	Current dens. [A/mm^2]	PM mass [kg]	Spec. power [kW/kg]	Power dens. [kW/L]	Eff. [%]	Goodness [N.m/$\sqrt{\text{W}_{\text{loss}}}$]
(a)	24	57.3	33.0	9.4	33.0	92.4	12.8
(b)	24	57.6	33.0	12.8	48.9	92.8	12.7
(c)	40	52.8	40.1	22.4	76.7	96.2	18.3
(d)	40	56.2	29.9	26.4	85.3	95.5	16.3

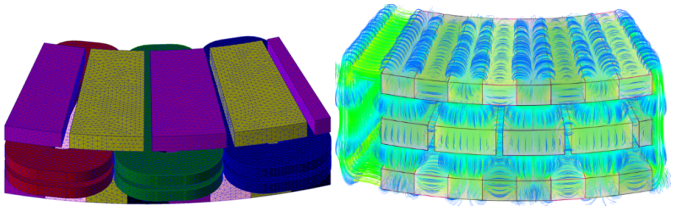

(a) (b)

Fig. 8. Three-dimensional FEA models utilizing matching and symmetry boundary conditions: (a) mesh plot and (b) 3D flux density distributions.

redundancy techniques, the use of specialized and additive materials, and incorporating high safety margins in the electromagnetic, electrical, and mechanical designs.

The multi-disk topologies employ the same stator structure as the single-disk coreless AFPM to enhance redundancy. Each topology in Fig. 5 features four sets of electrically isolated windings and four separate power electronic units, as illustrated in Fig. 7. Consequently, each stator contributes to one-fourth of the total power, effectively doubling the fault-tolerant capability compared to the single-disk machine. In topologies (a) and (c), the stators are not only electrically isolated but also magnetically decoupled, further improving fault-tolerant capability.

A fault in the rotor of the proposed coreless AFPM motors, such as permanent demagnetization of PMs due to a temperature rise, can significantly impact performance. If this fault occurs in one rotor of a single-disk coreless AFPM motor, the power output is reduced by half, assuming the other rotor remains operational. In multi-disk structures, the power reduction is less drastic. For topology (c), the power output retains 75% of the rated power, while design (d) maintains between 50% to 75% of the rated power.

To examine the performance of coreless AFPM motors in topologies (c) and (d) when a fault occurs in one of the rotors, the flux densities in the absence of one rotor must be calculated. Although AFPM machines present 3D challenges due to fringing and curvature effects, an unrolled 2D cylindrical model at the machine's average diameter can effectively estimate the airgap flux density. The calculations presented thus far were conducted using 3D FEA. Figure 8 illustrates an example of a 3D FEA model mesh and the resulting flux density distributions. Due to the $\frac{8\pi}{P}$ circumferential symmetry

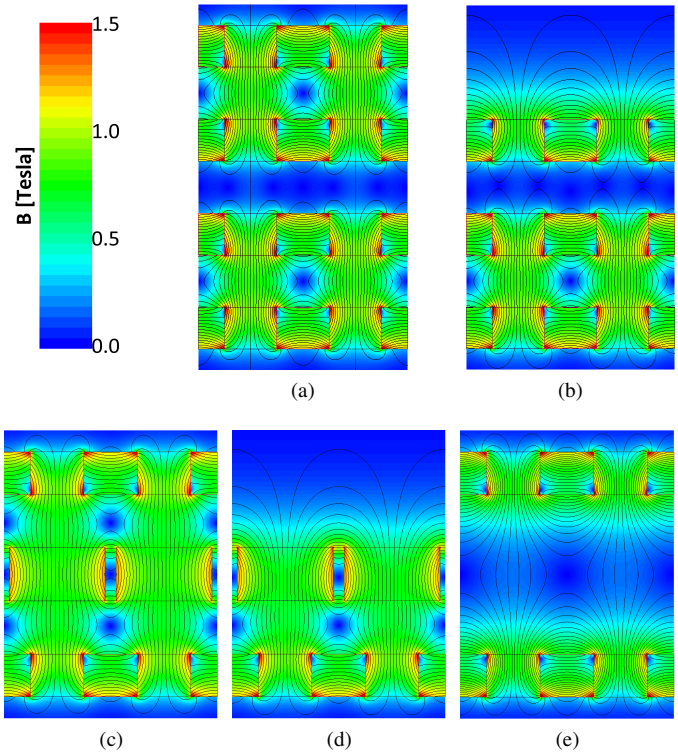

Fig. 9. Flux density distribution for topology (c) in case of (a) normal operation and (b) loss of one rotor, and for topology (d) when (a) normal operation, (b) loss of an outer rotor, and (c) loss of the inner rotor.

and half axial symmetry, appropriate matching and symmetry boundary conditions were applied.

The flux density distributions for the 2D equivalent models of topologies (c) and (d) under normal operation and in the case of losing one rotor due to demagnetization are depicted in Fig. 9. In topology (c), if one rotor fails, the other stack remains fully operational, while the faulty stack continues at half power. For design (d), the performance following an inner rotor fault depends on the M2M gap and the leakage flux.

While design (d) presents a higher specific power density than design (c), design (c) offers greater redundancy. The presence of two separate magnetic circuits in topology (c) enhances its modularity and fault tolerance. Furthermore, from a manufacturing and mechanical perspective, fabricating topology (d) is considerably more complex, and aligning all

the rotors present greater challenges compared to design (c).

VI. Conclusions

This paper presented several parametric studies on a single-disk coreless AFPM motor with two stators and Halbach array rotors for electric aircraft propulsion. The studies revealed that, aside from the outer diameter, the Halbach array pole number is the most crucial geometric parameter. The dimensions of the PM length, M2M gap, and rotor radial length depend on the pole pitch size, which is influenced by the pole number. Optimal specific power is achieved when these geometric parameters equal 0.4, 1, and 1 times the pole pitch, respectively.

Based on these results, multiple coreless AFPM motors with both single- and multi-disk topologies were proposed. To reduce magnetic coupling between the two stators of a single-disk motor, a topology with embedded rotor back iron between the stators was introduced. The 3D FEA results showed that with a disk-shaped rotor back iron, mutual inductances between different stators are eliminated, although this comes at the expense of lower specific power density.

Four different multi-disk coreless AFPM motor topologies were presented with surface PM and Halbach array rotors. For each rotor type, two multi-disk configurations were proposed: one with two single-disk motors mounted on a single mechanical shaft and another with three rotors and two stators. The Halbach array rotor designs exhibited significantly higher specific power and efficiency. Among these, the topology with three rotors and two stators achieved the highest specific power, while the configuration with two single-disk coreless AFPM motors on one shaft demonstrated superior efficiency and fault-tolerant capability.

Acknowledgment

This paper is based upon work supported by the National Aeronautics and Space Administration (NASA) through the University Leadership Initiative (ULI) #80NSSC22M0068. Any findings and conclusions expressed herein are those of the authors and do not necessarily reflect the views of NASA. The support of ANSYS Inc. and of University of Kentucky, the L. Stanley Pigman Chair in Power endowment is also gratefully acknowledged.

References

[1] R. Berger, "Hydrogen: A future fuel for aviation," 2024, accessed: 2024-07-15. [Online]. Available: https://www.rolandberger.com/en/Insights/Publications/Hydrogen-A-future-fuel-for-aviation.html

[2] S. Patel, E. Ragauss, J. Ahuja, J. C. Gladin, and D. N. Mavris, "Development of a regional blended wing body aircraft with distributed hybrid hydrogen-electric propulsion," in *AIAA SCITECH 2024 Forum*, 2024, p. 0282.

[3] M. Vatani, Y. Chulaee, A. Mohammadi, D. R. Stewart, J. F. Eastham, and D. M. Ionel, "On the optimal design of coreless AFPM machines with Halbach array rotors for electric aircraft propulsion," in *2024 IEEE Transportation Electrification Conference & Expo (ITEC)*. IEEE, 2024.

[4] M. Rosu, P. Zhou, D. Lin, D. M. Ionel, M. Popescu, F. Blaabjerg, V. Rallabandi, and D. Staton, *Multiphysics simulation by design for electrical machines, power electronics and drives*. John Wiley & Sons, 2017.

[5] J. F. Gieras, R.-J. Wang, and M. J. Kamper, *Axial flux permanent magnet brushless machines*. Springer Science & Business Media, 2008.

[6] F. Nishanth, J. Van Verdeghem, and E. L. Severson, "A review of axial flux permanent magnet machine technology," *IEEE Transactions on Industry Applications*, 2023.

[7] F. Nishanth, J. V. Verdeghem, and E. L. Severson, "Recent advances in analysis and design of axial flux permanent magnet electric machines," in *2021 IEEE Energy Conversion Congress and Exposition (ECCE)*, 2021, pp. 3745–3752.

[8] N. Taran, V. Rallabandi, G. Heins, and D. M. Ionel, "Coreless and conventional axial flux permanent magnet motors for solar cars," *IEEE Transactions on Industry Applications*, vol. 54, no. 6, pp. 5907–5917, 2018.

[9] Y. Chulaee, D. Lewis, M. Vatani, J. F. Eastham, and D. M. Ionel, "Torque and power capabilities of coreless axial flux machines with surface PMs and halbach array rotors," in *2023 IEEE International Electric Machines & Drives Conference (IEMDC)*. IEEE, 2023, pp. 1–6.

[10] D. Talebi, M. C. Gardner, S. V. Sankarraman, A. Daniar, and H. A. Toliyat, "Electromagnetic design characterization of a dual rotor axial flux motor for electric aircraft," *IEEE Transactions on Industry Applications*, vol. 58, no. 6, pp. 7088–7098, 2022.

[11] D. Talebi, C. Wiley, S. V. Sankarraman, M. C. Gardner, and M. Benedict, "Design of a carbon fiber rotor in a dual rotor axial flux motor for electric aircraft," *IEEE Transactions on Industry Applications*, pp. 1–9, 2024.

[12] K. Saviers, R. Regan, W. Zhao, A. Kuczek, A. Alahyari, Z. S. Du, J. A. Weibel, and J. Tangudu, "Stator prototype for a high current density electric motor: Assembly, evaluation, and testing," in *2023 IEEE Energy Conversion Congress and Exposition (ECCE)*. IEEE, 2023, pp. 1802–1808.

[13] Z. S. Du and J. Tangudu, "Novel compact 3-d PM machines for ultra high power density applications," in *2023 IEEE International Electric Machines & Drives Conference (IEMDC)*. IEEE, 2023, pp. 1–7.

[14] K. P. Duffy, "Optimizing power density and efficiency of a double-halbach permanent-magnet ironless axial flux motor," in *52nd AIAA/SAE/ASEE Joint Propulsion Conference*, 2016, p. 4712.

[15] F. Profumo, A. Tenconi, M. Cerchio, J. F. Eastham, and P. Coles, "Axial flux plastic multi-disc brushless pm motors: performance assessment," in *Nineteenth Annual IEEE Applied Power Electronics Conference and Exposition, 2004. APEC'04.*, vol. 2. IEEE, 2004, pp. 1117–1123.

[16] T. Bingham, M. Moore, T. De Caux, and M. Pacino, "Design, build, test and flight of the world's fastest electric aircraft," *IET Electrical Systems in Transportation*, vol. 12, no. 4, pp. 380–402, 2022.

[17] P. Virdi, W. Guo, L. Cattafesta, P. Cheetham, L. Cooley, J. Gladin, J. He, D. Ionel, C. Kim, H. Li *et al.*, "Liquid hydrogen storage and transfer-control system for integrated zero emission aviation (IZEA)," in *IOP Conference Series: Materials Science and Engineering*, vol. 1302, no. 1. IOP Publishing, 2024, p. 012024.

[18] M. Vatani, A. Mohammadi, D. Lewis, J. F. Eastham, and D. M. Ionel, "Coreless axial flux halbach array permanent magnet generator concept for direct-drive wind turbine," in *2023 12th International Conference on Renewable Energy Research and Applications (ICRERA)*. IEEE, 2023, pp. 612–617.

[19] "ARPA-E ASCEND 2022 annual meeting," 2022, publisher: US Department of Energy, Accessed: 2024-07-15. [Online]. Available: https://arpa-e.energy.gov/sites/default/files/2022-07/AML_2022_Annual_Mtg_ARPA-E_ASCEND.pdf